Bioorganic Chemistry 147 (2024) 107321

Contents lists available at ScienceDirect

Bioorganic Chemistry

journal homepage: www.elsevier.com/locate/bioorg

Discovery of two non-UDP-mimic inhibitors of O-GlcNAc transferase by screening a DNA-encoded library

Cyril Balsollier [a,b], Simon Bijkerk [a], Arjan de Smit [a], Kevin van Eekelen [a], Krištof Bozovičar [b], Dirk Husstege [a], Tihomir Tomašič [b], Marko Anderluh [b,*], Roland J. Pieters [a,*]

[a] Department of Chemical Biology & Drug Discovery, Utrecht Institute for Pharmaceutical Sciences, Utrecht University, Utrecht NL-3508 TB, The Netherlands
[b] Department of Pharmaceutical Chemistry, Faculty of Pharmacy, University of Ljubljana, Aškerčeva cesta 7, 1000 Ljubljana, Slovenia

ARTICLE INFO

Keywords:
O-GlcNAc transferase
Inhibition
DNA-encoded library

ABSTRACT

Finding potent inhibitors of O-GlcNAc transferase (OGT) has proven to be a challenge, especially because the diversity of published inhibitors is low. The large majority of available OGT inhibitors are uridine-based or uridine-like compounds that mimic the main interactions of glycosyl donor UDP-GlcNAc with the enzyme. Until recently, screening of DNA-encoded libraries for discovering hits against protein targets was dedicated to a few laboratories around the world, but has become accessible to wider public with the recent launch of the DELopen platform. Here we report the results and follow-up of a DNA-encoded library screening by using the DELopen platform. This led to the discovery of two new hits with structural features not resembling UDP. Small focused libraries bearing those two scaffolds were made, leading to low micromolar inhibition of OGT and elucidation of their structure–activity relationship.

1. Introduction

O-GlcNAcylation is an emerging topic in medicinal chemistry due to its involvement in cancer [1–3], diabetes [4–6] and Alzheimer's disease [7,8]. This intracellular post-translational modification has an impact on various biological pathways. O-GlcNAcylation is involved in bone marrow differentiation in perinatal bone growth [9], cell life cycle [10], autophagy [4], and protein activity [11]. O-GlcNAcylation is also involved in crosstalk with phosphorylation, adding to the complexity and impact of its role in human biology. O-GlcNAcylation involves only two enzymes: O-GlcNAc transferase (OGT) that transfers a β-*N*-acetyl-glucosamine moiety from UDP-GlcNAc to protein substrates, and O-GlcNAcase (OGA) that removes it. There are three isoforms of OGT with different subcellular localization. They have different lengths of their TPR domains. These *N*-terminal regions of the enzyme contain tetra-tricopeptide repeats (TPRs), consisting of 34 amino acids forming a pair of alpha-helixes that form a superhelix which mediates protein–protein interactions and substrate recognition [12,13]. The longest and the shortest isoforms known as ncOGT (110 kDa −13.5 TPRs) and sOGT (75 kDa −2.5 TPRs), are located in the nucleus and cytoplasm of human cells. The third variant is located in mitochondria, and it is known as mOGT (103 kDa −9.5 TPRs) [14].

While for OGA inhibition one inhibitor is in clinical trials for tauopathies and Alzheimer's disease [15,16], OGT inhibition has proven more challenging. Known OGT inhibitors include uridine derivatives [17], and bisubstrate inhibitors [18–20] that lack cell permeability. Virtual screening and compound screening resulted in different uridine mimics such as benzo-indolinone, benzo-thiazolone, benzo-oxazolone, benzo-imidazolinone [21,22], quinolones [23], and notably quinolone-4-sulfonamides. The last group contains the most potent OGT inhibitor to date, OSMI-4 [24,25]. Apart from OSMI-4, with a K_d of 8 nM, other compounds showed mostly micromolar activity (defined by their relative inhibition constants IC_{50}) [26–28]. While OSMI-4 has good *in vitro* potency, its cellular activity is two orders of magnitude lower and has to be applied in an ester form to allow cellular permeability, while its cleavage is not required for on-target activity [29]. Clearly, there is a need to find new OGT inhibitors.

DNA-Encoded Libraries (DEL) can contain many compounds with unique DNA tags as identifiers. The technology uses the combinatorial synthesis method to build up large libraries [30]. Since 2002 the DEL technology is a tool in medicinal chemistry for screening purposes where identification of hits is facilitated by the DNA tag [31–37]. Here we report on the discovery of new non-UDP mimetic OGT inhibitors by using the DELopen platform, a DEL available to academic users by WuXi

* Corresponding authors.
E-mail addresses: Marko.Anderluh@ffa.uni-lj.si (M. Anderluh), R.J.Pieters@uu.nl (R.J. Pieters).

https://doi.org/10.1016/j.bioorg.2024.107321
Received 29 January 2024; Received in revised form 26 March 2024; Accepted 28 March 2024
Available online 29 March 2024

AppTec. A small library of analogues was prepared and tested *in vitro* against OGT. Computer docking provided a direction for future optimization of these molecules.

2. Results and discussion

2.1. DNA-encoded library screening

For screening a DNA-encoded compound library, we used the DELopen service [38]. In their setup 4.4 billion unique molecules were screened against three immobilized isoforms of OGT. Using different isoforms allowed us to select molecules that would only bind to the active site or possibly allosteric sites of the enzyme part, the common part of the three OGT isoforms. The DELopen assay was performed as described in the general protocol provided by the company. His-tagged enzymes were immobilized on magnetic Ni-NTA beads and were subsequently incubated with the DELopen library. After washing unbound compounds, bound compounds were released by heat. These were enriched with more immobilized protein in two further rounds of selection. After performing the affinity selection, the manufacturer WuXI AppTec performed the sequencing and provided a hitlist from which 5 compounds that bound to the 3 isoforms were selected for purchase and further resynthesis. Two of these compounds were identified as micromolar hits against OGT: compounds **10207** and **10115** (Fig. 1).

2.2. Analogues of compound *10207*

To validate the identified hits and to identify the important parts of the molecules for the binding, synthesis of analogues was performed. The synthesis started with a Hantzsch thiazole synthesis between 4-bromo-1,1-dimethoxybutan-2-one (**1**), and 4-bromobenzothioamide (**2**) giving the expected thiazole **3** (Fig. 2). The aldehyde was then deprotected yielding **4** to undergo a Wittig-Horner reaction to install the *trans* double bond. Subsequent hydrolysis of the ester yielded building block **5**. The second building block started with a peptide coupling between Boc-protected tryptophan (**6**) and ethyl *(R)*-2-amino-2-cyclohexylacetate (**7a**) to form **8a**. Boc removal provided the second building block **9a**. Similarly, phenylglycine derivatives **8b** and **9b** were synthesized. Building blocks **5** and **9a-b** were connected by peptide coupling to yield **10** and **12.** Compound **10** was subsequently saponified to form the free carboxylic acid **11**. The inhibition assay [39] gave IC_{50}'s of 67 μM and 51 μM respectively for ester (**10**) and the carboxylic acid (**11**) (Fig. 3). These inhibitory potencies are close to the determined IC_{50} value of **10207** (67 μM), which bears the amidomethyl terminus. The fact that the carboxylic acid, ester or amide makes little difference to the inhibition is consistent with the notion that this part of the molecule is the attachment point of the original DNA label during the screening. The IC_{50} of the small library of **10207** fragments gave hints on which parts of the molecules are the most important for the binding. The smallest substructure, compound **5**, showed no inhibition of OGT at 300 μM. However, removing this part from compound **10**, thus creating compound **9a**, dropped the inhibition from an IC_{50} of 51 μM for **10** to an IC_{50} of 299 μM for **9a**. These data indicate that while **5** showed no detectable binding, once linked to **9a**, its features do contribute to it. Concerning compound **12**, replacing the cyclohexane ring with a benzene ring, resulted in a substantial drop of the inhibition compared to **10**, giving an IC_{50} of 334 μM for **12.**

2.3. Analogues of compound *10115*

To synthesize **10115** and analogues thereof, two building blocks were needed: building block **16**, bearing both the furan and the 5-phenylnicotinic acid, and building block **20** with the biphenyl moiety linked to the stereocenter (Fig. 4.). The synthesis of building block **16** started from carboxylic acid **13**, which was converted to its tert-butyl ester **14**. This compound was subjected to a Suzuki reaction with furan-2-yl boronic acid to yield **15** and the removal of the tert-butyl ester gave the free carboxylic acid **16.** For the synthesis of building block **20** we started with [1,1′-biphenyl]-4-carbonyl chloride and *N,O*-dimethylhydroxylamine to form Weinreb amide **17**. Subsequently, a reduction with $LiAlH_4$ was performed to give the aldehyde **18**. The latter was reacted with malonic acid in a Rodionov reaction giving the unnatural racemic β-amino acid **19** followed by ethyl ester formation to yield **20**. The two building blocks were then conjugated together by amide bond formation giving ethyl ester **21**, which was subjected to aminolysis to yield the methylamide **10115**.

Variations of the building blocks were introduced. The role of the furan in the interaction with OGT was addressed by using the analogous bromo building block **13** instead of **16**. For building block **20**, two points of investigation were selected. Firstly, the second phenyl was replaced by a bromine in **22** or a hydrogen in **23**. Secondly both enantiomers of **23** were used (Fig. 5). Peptide coupling of the various building blocks yielded **24**–**27.**

This library was tested along with **10115** and **21** in the OGT inhibition assay [39](Fig. 6.). The IC_{50} values for **10115** (31 μM) and **21** (52 μM) showed that the terminal part of the molecule has no significant impact on the inhibitory potency, again consistent with the notion that this part was linked to the DNA in the original DNA-encoded library and

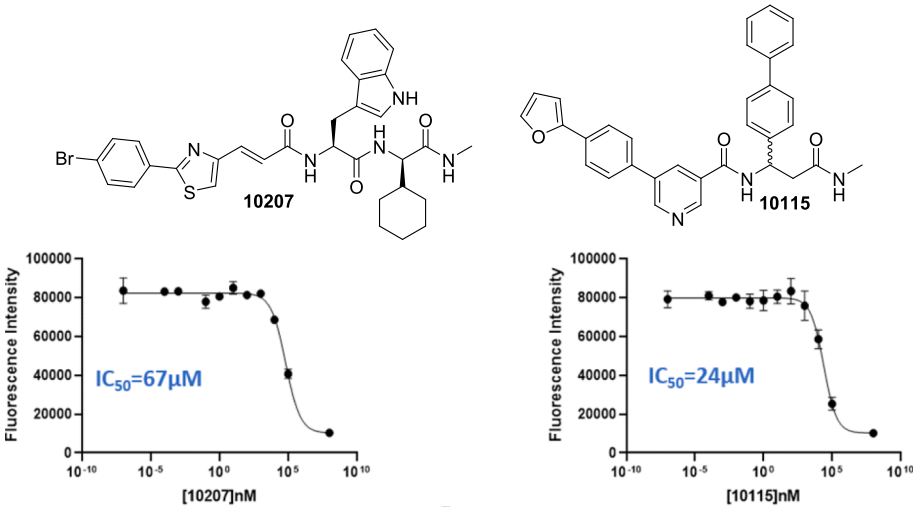

Fig.1. Structure and IC_{50} of the hits **10207** and **10115.**

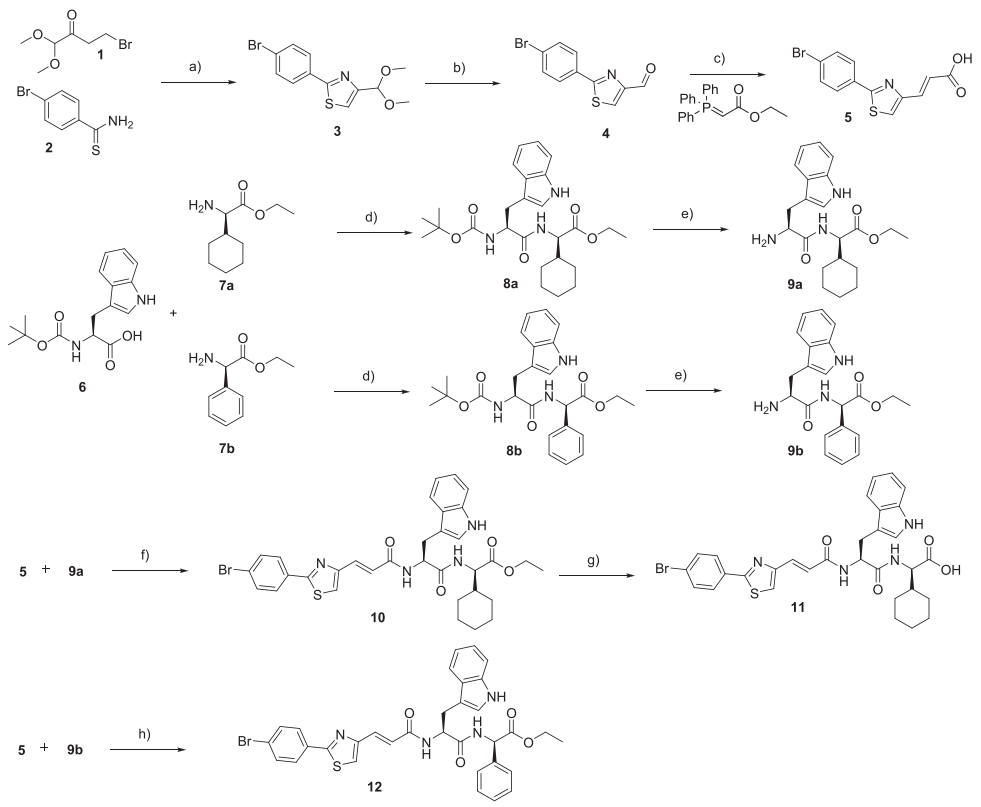

Fig. 2. Synthesis of **10207** analogues. Reagents and conditions: (a) EtOH, Δ, 83 %; (b) HCl, H_2O, quant.; (c) 1) Toluene, r.t. → 60 °C; 2) NaOH, EtOH, H_2O, 85 % over 2 steps; (d) DCM, DCC, DMAP, 92 % for **8a**, 78 % for **8b**; (e) 40 % HCl in dioxane, 83 % for **9a**, quant for **9b**; (f) HATU, DMF, 82 % for **10**, 84 % for **12** (g) DCM, LiOH, quantitative.

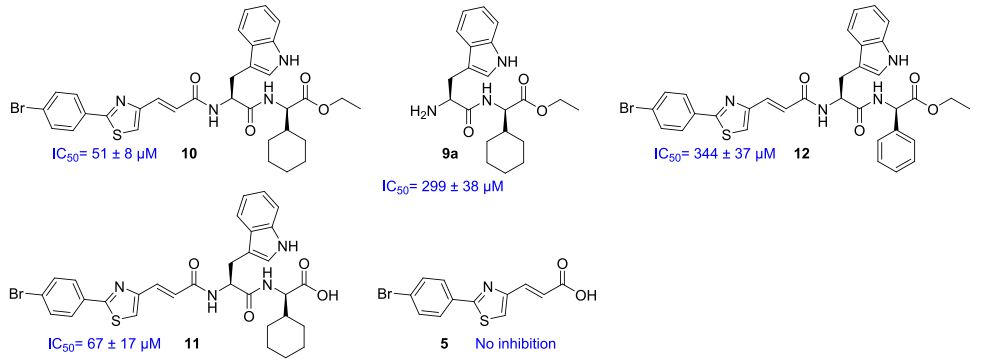

Fig. 3. OGT inhibition assay results of the small library derived from **10207**.

therefore less likely to be involved in binding. Concerning compound **21** (IC_{50} 52 µM) versus **26** (IC_{50} 197 µM), the results indicated that the furan moiety plays an important role in the binding since as soon as it is removed, as for **26**, there is a significant drop in activity. Comparing **24** with **25** leads to the same conclusion. Whether the biphenyl has an impact on the potency is less clear. When comparing the potency of **21** to **24**, the biphenyl is a bit worse than the bromophenyl. On the other hand, comparing **25** to **26** shows a moderate advantage of the biphenyl. The stereochemistry of the β-amino acid was shown to play a role in the binding as *S*-enantiomer **27b** (IC_{50} 47 µM) inhibits more potently than *R*-enantiomer **27a** (IC_{50} 337 µM).

2.4. Molecular docking

The inhibition results were rationalized with docking studies performed by using the OpenEye/FRED docking software. A likely binding pose, seen most often among the highest scoring poses for **10207** is shown in Fig. 7A. The three branches, i.e the tryptophan, the thiazole-bromophenyl and the cyclohexyl group were roughly in the same position in the binding pocket in most of the highly scoring binding poses.

The pose did not feature the usual uridine or uridine mimic (of UDP- or UDP-GlcNAc, see Fig. 7C) two "hinge" hydrogen bonds formed with both carbonyl and amino residues of Ala896. Besides various close hydrophobic contacts, prominent hydrogen bonds include the two amide carbonyls and the indole NH were suggested by the software. Interestingly, here one or possibly two of the amide carbonyls of **10207** bind to the Gln839 primary amide of the protein, while this residue binds to the diphosphate part of UDP (Fig. 7C) or UDP-GlcNAc during catalysis. Further optimizations of this compound class may come from extending the molecule to the uridine binding pocket e.g. through replacement of the thiazole by a tri-substituted 5-member ring.

Similarly, docking was performed for the *S*-enantiomer of **10115**, i.e.

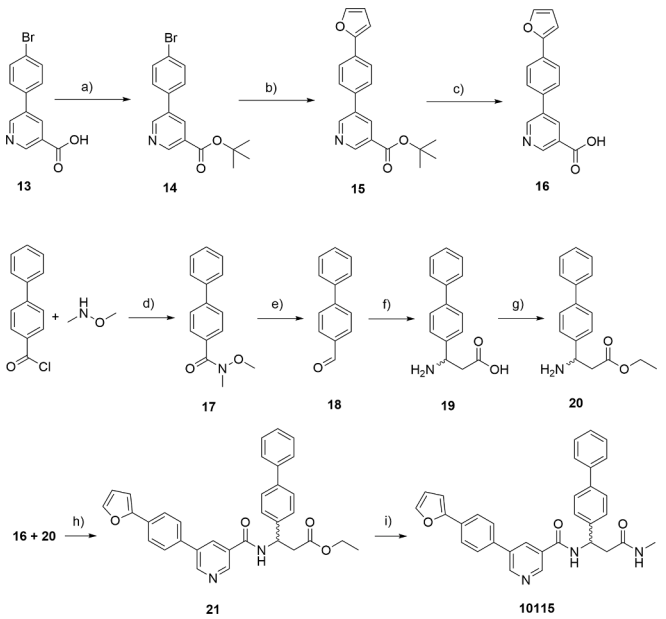

Fig. 4. Synthesis of **10115**. Reagents and conditions a) Boc_2O, DMAP, THF, Δ, 16 h, 90 %; b) furan-2-yl boronic acid, THF/H_2O, $Pd(dppf)Cl_2$, 16 h, 27 %; c) DCM, TFA, 0 °C to 21 °C, 72 h, 94 %; d) Et_3N, DCM, 82 %; e) $LiAlH_4$, THF, 93 %; f) malonic acid, NH_4OAc, EtOH, reflux, 35 %; g) $SOCl_2$, EtOH, reflux; h) DMF, HATU, DiPEA, 21 °C, 48 h 72 %; i) 40 % $MeNH_2$ in MeOH, MW 80 °C, 3 h, 97 %.

the preferred enantiomer of this compound class based on the observed superiority of **27b** over **27a**. A prominent pose is shown in Fig. 7B. Again, the molecule features three branches, in this case the biphenyl branch, the pyridine-phenyl-furan branch and finally the methylamide. In certain poses two branches are switched. In the pose shown, the pyridine nitrogen, and the amide carbonyls are engaged in hydrogen bonds with OGT. Additionally, there are hydrophobic contacts between the ligand and the protein and there is overall good shape complementarity. Similar to the case of **10207**, also here the docking does not show any indication of the "hinge" hydrogen bonds of the compound with Ala896, i.e. the designated uridine binding site. This compound thus also binds in a novel binding mode. Further potency enhancement may involve taking advantage of the nearby uridine binding site.

3. Conclusions

In our study, a DNA-encoded library allowed us to identify two hits as OGT inhibitors. Both hits are from different chemotypes than previously published OGT inhibitors and both have an IC_{50} in the low micromolar range. Our study focused on the synthesis of analogues of both hits to decipher molecular fragments that are important for binding. Together with molecular docking studies, the data generated within this work elucidates novel OGT inhibitors and points to future structural modifications that could lead to even higher potency. Apart from being promising hits, the new chemotypes do not rely on UDP mimicking moieties. Future work could be directed towards more potent non-UDP based OGT inhibitors to open new ways to study O-GlcNAcylation inhibition.

4. Experimental

4.1. General

Chemicals were obtained from commercial sources and were used without further purification unless noted otherwise. Bromo-1,1-dimethoxybutan-2-one was purchased from Enamine with a purity of 80 %. The compounds 5–4-bromophenyl nicotinic acid **(14)**, ethyl-*(R)*-3-amino-3-phenylpropanoate **(24a)** and, ethyl-*(S)*-3-amino-3-phenylpropanoate (**24b)** were purchased from Accela biotech. Bodipy Fluorescent Labeled UDP-GlcNAc (BFL-UDP-GlcNAc) was obtained from prof. D. J. Vocadlo (Simon Fraser University). Other compounds were purchased from Sigma-Aldrich and Thermo Fisher except stated otherwise. Solvents were purchased from Biosolve (Valkenswaard, The Netherlands). All moisture-sensitive reactions were performed under a nitrogen atmosphere. Thin-layer chromatography (TLC) was performed on Merck precoated Silica 60 plates. Spots were visualized by UV light, 10 % H_2SO_4 in MeOH, $KMnO_4$, or ninhydrine stain. Microwave reactions were carried out in a Biotage microwave Initiator (Uppsala, Sweden). The microwave power was limited by temperature control once the desired temperature was reached. Sealed vessels 10–20 mL were used. Lyophilization was performed on a Christ Alpha 1–2 apparatus. Preparative HPLC of final compounds were done on Shimadzu LC-8A preparative liquid chromatograph system with a Gilson 215 fraction collector on a C18 column on a water/acetonitrile system. HPLC analytics were run on Shimadzu LC-10AT system on a C18 column paired with the preparative column. The used buffers were H_2O 0.1 % TFA (buffer A, pH 4.4) and CH_3CN 0.1 % TFA (buffer B). Also, UV absorption was measured at 254 nm and 214 nm. Runs were performed using a standard protocol: 0 to 100 % gradient buffer B in 90 min. ^1H and ^{13}C NMR were performed on an Agilent 400 MR or a Bruker 600 UtraShield spectrometer. Chemical shifts (δ) are reported in ppm relative to residual solvent signals, and peak assignments were established based on additional $^1H-^1H$ COSY and $^1H-^{13}C$ HSQC experiments. High-resolution mass spectrometry (HRMS) analysis was performed using an ESI-QTOF II spectrometer.

4.2. OGT inhibition assay [39]

OGT reactions were carried out in a 25-μL final volume, containing 2.8 μM glycosyl donor BFL-UDP-GlcNAc, 1.6 μM purified full-length OGT, 9.2 μM glycosyl acceptor HCF-1 Serine in OGT reaction buffer (1 × PBS pH 7.4, 1 mM DTT, 12.5 mM $MgCl_2$). Reactions were incubated at room temperature for 1 h, in the presence of different concentrations

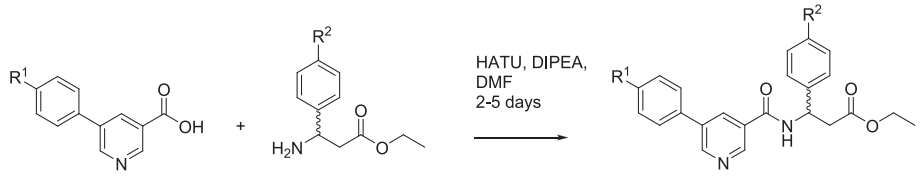

13: R^1 = Br
16: R^1 = Furan-2-yl

20: R^2 = Phenyl
22: R^2 = Br
23a: R^2 = H (R)
23b: R^2 = H (S)

24: R^1 = Furan-2-yl; R^2 = Br; 39%
25: R^1 = Br; R^2 = Br; 37%
26: R^1 = Br; R^2 = Phenyl; 40%
27a: R^1 = Furan-2-yl; R^2 = H; (R) 72%
27b: R^1 = Furan-2-yl; R^2 = H; (S) 72%

Fig. 5. Synthesis of **10115** derivatives.

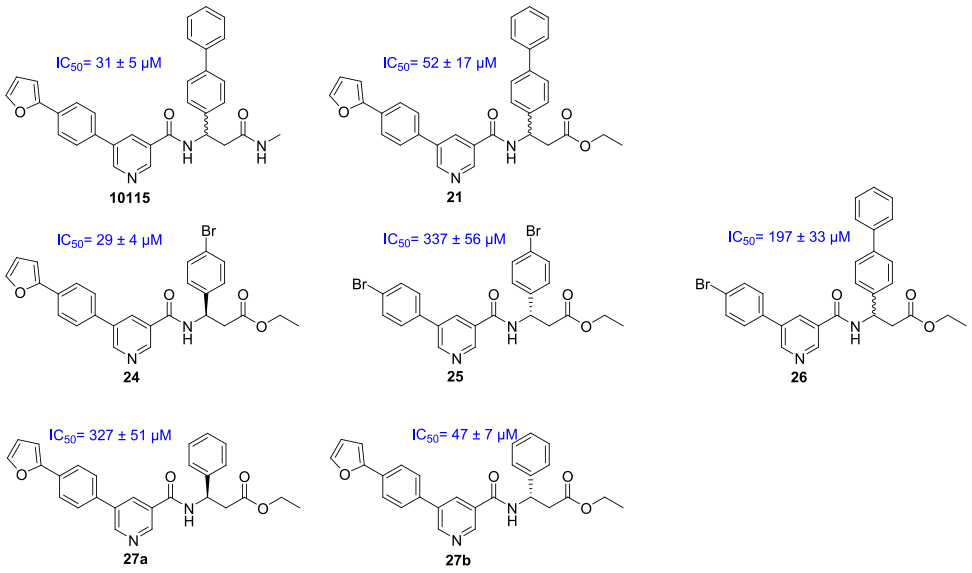

Fig. 6. OGT inhibition IC_{50} values of the 10115-based library.

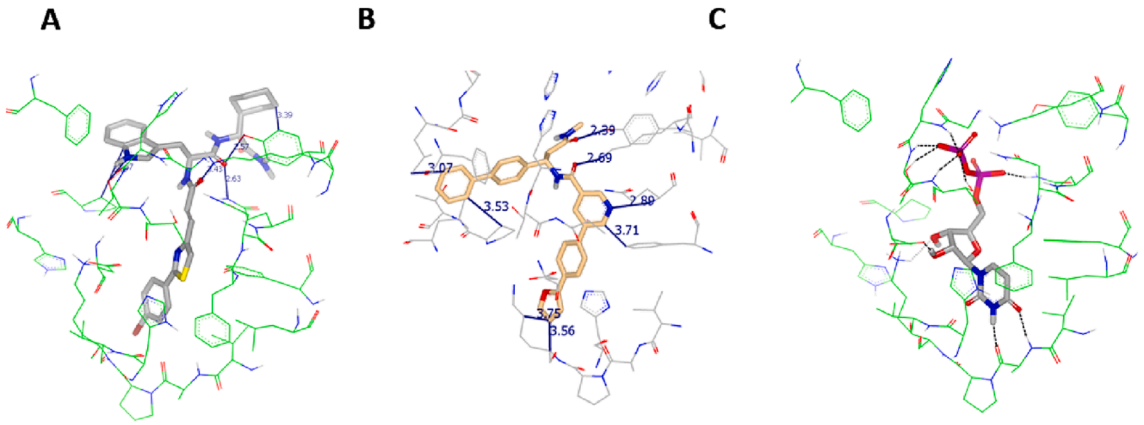

Fig. 7. Potential binding poses of compounds 10207 (A) and 10115 (B), and UDP, the original ligand in the X-ray structure, PDB ID: 4 N39 [40](C).

of inhibitor (the inhibitors were preincubated with OGT for at least 5 min). The reactions were then stopped by the addition of UDP at a final concentration of 10 mM, followed by Nanolink magnetic streptavidin beads (3 μL). After incubation at room temperature for 30 min, the beads were immobilized on a magnetic surface and washed thoroughly with PBS-tween 0.01 %. Finally, the beads were resuspended in PBS-tween 0.01 % and transferred to a microplate for endpoint fluorescence measurement. Fluorescence was read at Ex/Em 485/530 with a POLARstar® Omega microplate reader (BMG LABTECH). The data were plotted with GraphPad prism software, version 8, [Inhibitor] vs. response-variable slope. All IC_{50} were measured in two independent experiments. Each experiment was performed in 3 technical replicates.

4.3. Docking

For docking with FRED software [41,42] (Release 4.1.1.0, OpenEye Scientific Software, Inc., Santa Fe, NM, USA; **www.eyesopen.com**), the UDP-GlcNAc binding site in OGT (PDB entry: 4 N39 [40]) was prepared using MAKE RECEPTOR (Release 4.1.1.0, OpenEye Scientific Software, Inc., Santa Fe, NM, USA; **www.eyesopen.com**). For "Cavity detection", a slow and effective "Molecular" method was used for the detection of binding sites. The grid box around UDP in the OGT crystal structure was generated automatically. The outer contour of the grid box was calculated using the "Balanced" settings for the "Site Shape Potential" calculation. The box was then adjusted to fully cover the outer contour, with no sides of the box limiting the contour size, resulting in a box of 19.33x26.67x19.33 Å (9967 $Å^3$) with a 1945 $Å^3$ outer-contour in it. The small molecule library, was prepared by Tautomers and pKaTyper (QUACPAC release 2.1.3.0, OpenEye Scientific Software, Inc., Santa Fe, NM, USA; **www.eyesopen.com**). For Tautomers, "stereo" was set to "EverSampled", "pkanorm" set to false. For pKaTyper default settings were used. Conformers were generated with OMEGA (Release 4.1.2.0, OpenEye Scientific Software, Inc., Santa Fe, NM, USA; **www.eyesopen.com**). Classic mode was used with "flipper" and "strictfrags" enabled and "maxconfs" set to 8000. The conformers were docked at the prepared UDP-GlcNAc-binding site of OGT using FRED. The "dock-resolution" was set to high, "numposes" to 100. The ten best ranked poses for each compound were inspected visually and used for analysis and representation.

4.4. Synthesis

4.4.1. 2-(4-bromophenyl)-4-(dimethoxymethyl)thiazole) (3)

4-bromo-1,1-dimethoxybutan-2-one (750 mg, 3.96 mmol) and 4-bromobenzothioamide (856 mg, 3.96 mmol) were mixed in EtOH (100 mL) and heated under reflux for 3 h. The reaction mixture was concentrated and purified by silica gel chromatography using a gradient from 0 to 30 % EtOAc/PE. The fractions were evaporated under reduced pressure

giving 929 mg of a yellow pale solid at 75 % yield. ^{1}H NMR (400 MHz, $CDCl_3$) δ 7.86–7.81 (m, 2H), 7.58–7.52 (m, 2H), 7.42 (d, J = 0.8 Hz, 1H), 5.68 (d, J = 0.8 Hz, 1H), 1.27 (t, J = 7.1 Hz, 6H); the data are in accordance with those reported [43].

4.4.2. 2-(4-bromophenyl)thiazole-4-carbaldehyde (4)

Compound **3** (929 mg, 2,97 mmol) was dissolved in an HCl solution (20 mL, 4 M) and stirred for 2 h at 21 °C forming a precipitate. DCM was added to the mixture dissolving the precipitate. Liquid-liquid extraction was performed by extracting the water layer two times with DCM (20 mL). The organic layer was dried with Na_2SO_4 and evaporated under vacuum giving 650 mg (2.44 mmol) of yellow oil with 82 % yield. ^{1}H NMR (400 MHz, $CDCl_3$) δ 10.09 (s, 1H), 8.18 (s, 1H), 7.88 (d, J = 8.6 Hz, 2H), 7.62 (d, J = 8.6 Hz, 2H). NMR date were accordance with the literature [43].

4.4.3. (E)-3-(2-(4-bromophenyl)thiazol-4-yl)acrylic acid (5)

Compound **4** (839 mg, 3.1 mmol) was dissolved in toluene. After complete dissolution, ethyl 2-(triphenyl-λ5-phosphaneylidene)acetate (1.361 g, 3.9 mmol) was added to the reaction mixture. The resulting mixture was then warmed up to 80 °C for 1.5 h. The reaction mixture was concentrated and purified through silica column chromatography using a gradient from 0 to 20 % EtOAc in PE. ^{1}H NMR (400 MHz, $CDCl_3$) δ 7.89–7.83 (m, 2H), 7.65–7.56 (m, 3H), 7.42 (d, J = 0.5 Hz, 1H), 6.87 (d, J = 15.5 Hz, 1H), 4.28 (q, J = 7.1 Hz, 2H), 1.34 (t, J = 7.1 Hz, 3H). The product from the column was dissolved in EtOH and a large excess of NaOH was added. The solution was then heated at reflux for 16 h. After evaporating the solvent the obtained solid was dissolved in distilled water and acidified with HCl (1 M) to pH = 1, creating a white precipitate. The precipitate was filtered, dissolved in acetone, washed with Na_2SO_4 and dried under vacuum giving 540 mg of a greyish solid with a yield of 85 % over 2 steps. ^{1}H NMR (400 MHz, DMSO-d_6) δ 12.51 (s, 1H), 8.16 (s, 1H), 8.00–7.89 (m, 2H), 7.73 (d, J = 8.6 Hz, 2H), 7.61 (d, J = 15.6 Hz, 1H), 6.67 (d, J = 15.6 Hz, 1H). ^{13}C NMR (151 MHz, DMSO-d_6) δ 167.11, 152.47, 136.53, 132.78, 132.43, 132.18, 128.81, 128.65, 128.31, 124.59, 124.43, 121.66. HRMS (ESI/Q-TOF) m/z: $[M + H]^+$ Calcd for $C_{12}H_8BrNO_2S$ 309.9469; Found 309.9471.

4.4.4. Ethyl (R)-2-((S)(S)-2-((tert-butoxycarbonyl)amino)-3-(1H-indol-3-yl)propanamido)-2-cyclohexylacetate (8a)

(tert-butoxycarbonyl)-L-tryptophan (304 mg, 1 mmol) was dissolved in DMF (25 mL). HATU (229 mg, 1.1 mmol) was added to the mixture along with DiPEA (78 mg, 0.6 mmol) and the reaction mixture was stirred at 21 °C. After 20 min Ethyl *(R)*-2-amino-2-cyclohexylacetate (185 mg, 1 mmol) was added dropwise to the mix and the reaction was stirred for 48 h at 21 °C. The reaction mixture was concentrated and 2-times co-evaporated using toluene followed by column chromatography (3:7 PE: EtOAc) giving 353 mg of a brown oil with a yield of 75 %. ^{1}H NMR (600 MHz, $CDCl_3$) δ 8.71 (s, 1H), 7.52 (d, J = 7.9 Hz, 1H), 7.38–7.33 (m, 1H), 7.18–7.04 (m, 4H), 4.35 (t, J = 6.9 Hz, 1H), 4.19 (dd, J = 8.0, 5.6 Hz, 1H), 4.13 (qd, J = 7.1, 1.2 Hz, 2H), 3.35 (dd, J = 15.0, 6.6 Hz, 1H), 3.26 (dd, J = 15.0, 7.1 Hz, 1H), 1.69–1.60 (m, 3H), 1.55 (s, 1H), 1.43 (t, J = 11.7 Hz, 2H) 1.37 (s, J = 8.5 Hz, 9H) 1.27 (t, J = 7.1 Hz, 3H), 1.11 (ddt, J = 16.3, 12.9, 6.5 Hz, 2H), 0.99 (dddd, J = 16.3, 12.8, 8.0, 3.5 Hz, 1H), 0.88 (td, J = 12.8, 3.9 Hz, 1H), 0.83 (td, J = 12.7, 3.8 Hz, 1H).

4.4.5. Ethyl (R)-2-((S)-2-((tert-butoxycarbonyl)amino)-3-(1H-indol-3-yl) propanamido)-2-phenylacetate (8b) was prepared according to the same procedure as shown for 8a

Yield 84 %; ^{1}H NMR (600 MHz, $CDCl_3$) δ 8.1 (s, 1H), 7.32–7.25 (m, 3H), 7.10–6.95 (m, 3H), 6.95–6.77 (m, 3H), 5.21 (td, J = 7.9, 5.5 Hz, 2H), 4.00 (m, 2H), 3.28–3.14 (m, 1H), 3.20 (dd, J = 14.5, 8.0 Hz, 1H), 1.25 (s, J = 8.3 Hz, 9H), 1.00(t, J = 7.1 Hz, 3H).

4.4.6. Ethyl (R)-2-((S)-2-amino-3-(1H-indol-3-yl)propanamido)-2-cyclohexylacetate (9a)

8a (235 mg, 0.6 mmol) was dissolved in 40 % HCl in dioxane and stirred at 21 °C for 2 h. The solvent was evaporated and the remaining oil was purified on a silica gel column with 30/70 PE/EtOAc and further on PREP-HPLC giving 186 mg of final product (83 %).^{1}H NMR (600 MHz, $CDCl_3$) δ 8.71 (s, 1H), 7.52 (d, J = 7.9 Hz, 1H), 7.38–7.33 (m, 1H), 7.18–7.04 (m, 4H), 4.35 (t, J = 6.9 Hz, 1H), 4.19 (dd, J = 8.0, 5.6 Hz, 1H), 4.13 (qd, J = 7.1, 1.2 Hz, 2H), 3.35 (dd, J = 15.0, 6.6 Hz, 1H), 3.26 (dd, J = 15.0, 7.2 Hz, 1H), 1.69–1.60 (m, 3H), 1.55 (s, 1H), 1.43 (t, J = 11.7 Hz, 2H), 1.27 (t, J = 7.1 Hz, 3H), 1.11 (ddt, J = 16.3, 12.9, 6.5 Hz, 2H), 0.99 (dddd, J = 16.4, 12.8, 8.0, 3.5 Hz, 1H), 0.88 (td, J = 12.8, 3.9 Hz, 1H), 0.83 (td, J = 12.7, 3.8 Hz, 1H).^{13}C NMR (151 MHz, $CDCl_3$) δ 171.18, 168.61, 136.38, 126.73, 124.99, 122.35, 119.75, 118.17, 111.68, 106.97, 61.57, 58.02, 53.75, 40.36, 29.07, 28.04, 27.34, 25.74, 25.62, 14.09. HRMS (ESI/Q-TOF) m/z: $[M + H]^+$ Calcd for $C_{21}H_{29}N_3O_3$ 372.2209; Found 372.2284. HPLC Ret. time 28.69 min, purity 99.2 % (254 nm) 99.1 % (214 nm).

4.4.7. Ethyl (R)-2-((S)-2-amino-3-(1H-indol-3-yl)propanamido)-2-phenylacetate (9b) was prepared according to the same procedure as shown for 9a starting from 8b

Yield 78 %. ^{1}H NMR (600 MHz, $CDCl_3$) δ 8.06 (s, 1H), 7.36–7.29 (m, 3H), 7.15–7.07 (m, 3H), 6.91–6.77 (m, 3H), 5.01 (td, J = 7.9, 5.5 Hz, 2H), 4.10 (ddq, J = 46.8, 10.8, 7.1 Hz, 2H), 3.37–3.32 (m, 1H), 3.20 (dd, J = 14.5, 8.0 Hz, 1H), 1.15 (t, J = 7.1 Hz, 3H).

4.4.8. Ethyl-(R)-2-((S)-2-((E)-3-(2-(4-bromophenyl)thiazol-4-yl) acrylamido)-3-(1H-indol-3-yl)propanamido)-2-cyclohexylacetate (10)

Compound **5** (20 mg, 0.064 mmol) was dissolved in DMF (10 mL) along with HATU (27 mg, 0.0704 mmol). After stirring for 20 min, compound **9a** (24 mg, 0.064 mmol) in DMF was added dropwise to the mix and the reaction was stirred for 48 h at 21 °C. The reaction mixture was concentrated and 2-times co-evaporated using toluene followed by column chromatography (3:7 PE: EtOAc) followed by preparative HPLC giving 35 mg of a yellowish oil with a yield of 82 %. ^{1}H NMR (600 MHz, $CDCl_3$) δ 8.19–8.14 (m, 1H), 7.85–7.80 (m, 2H), 7.68 (d, J = 7.9 Hz, 1H), 7.60–7.57 (m, 2H), 7.40 (s, 1H), 7.37–7.33 (m, 1H), 7.19 (ddd, J = 8.1, 7.0, 1.1 Hz, 1H), 7.16–7.11 (m, 3H), 6.93 (d, J = 15.1 Hz, 1H), 6.54 (d, J = 8.4 Hz, 1H), 5.04–4.93 (m, 1H), 4.34 (dd, J = 8.4, 5.3 Hz, 1H), 4.09 (qd, J = 7.2, 1.6 Hz, 2H), 3.36 (dd, J = 14.6, 5.7 Hz, 1H), 3.24 (dd, J = 14.6, 8.1 Hz, 1H), 1.67 (ddt, J = 15.4, 6.2, 3.4 Hz, 3H), 1.61–1.52 (m, 2H), 1.45 (d, J = 12.0 Hz, 1H), 1.31–1.27 (m, 1H), 1.26 (s, 4H), 1.23 (t, J = 7.1 Hz, 3H), 1.14 (tt, J = 12.9, 3.5 Hz, 2H), 1.05–0.98 (m, 1H), 0.93–0.85 (m, 2H). ^{13}C NMR (151 MHz, $CDCl_3$) δ 171.70, 170.90, 167.56, 166.79, 152.57, 136.26, 134.25, 132.24, 131.98, 128.18, 127.27, 124.97, 123.52, 122.40, 122.37, 121.65, 119.93, 118.67, 111.26, 110.01, 61.41, 57.48, 54.44, 40.78, 29.73, 29.25, 28.56, 28.08, 25.86, 25.79, 14.12. HRMS (ESI/Q-TOF) m/z: $[M + H]^+$ Calcd for $C_{33}H_{35}BrN_4O_4S$ 663,1562; Found 663,1641. HPLC Ret.time 41.8 min, purity 92 % (254 nm) 88 % (214 nm).

4.4.9. (R)-2-((S)-2-((E)-3-(2-(4-bromophenyl)thiazol-4-yl)acrylamido)-3-(1H-indol-3-yl)propanamido)-2-cyclohexylacetic acid (11)

Compound **10** (33 mg, 0,05 mmol) was dissolved in DCM (10 mL) and cooled to 4 °C before adding a LiOH solution (1 M, 0.5 mmol, 0.5 mL). The reaction was stirred for 3 h at 4 °C then DCM was removed under reduced pressure and the residue was partitioned between water and EtOAc. The aqueous layer was acidified with HCl until pH 4 and extracted with EtOAc)(10 mL). The organic phases were combined, dried over Na_2SO_4 and concentrated, giving 30 mg of an off-white solid in quantitative yield. ^{1}H NMR (600 MHz, DMSO-d_6) δ 10.86 (d, J = 2.4 Hz, 1H), 8.54 (d, J = 8.3 Hz, 1H), 8.20 (d, J = 8.4 Hz, 1H), 8.06 (s, 1H), 8.01–7.94 (m, 1H), 7.86–7.80 (m, 1H), 7.74 (d, J = 8.0 Hz, 1H), 7.45 (d, J = 15.3 Hz, 1H), 7.24 (d, J = 2.4 Hz, 1H), 7.13 (ddd, J = 8.2, 7.0, 1.2 Hz, 1H), 7.07–7.02 (m, 1H), 4.87 (ddd, J = 10.0, 8.3, 4.2 Hz, 1H), 4.25

(dd, $J = 8.4$, 6.2 Hz, 1H), 3.23 (dd, $J = 14.9$, 4.1 Hz, 1H), 3.03 (dd, $J = 14.9$, 10.0 Hz, 1H), 1.85–1.73 (m, 2H), 1.72–1.63 (m, 2H), 1.39–1.06 (m, 7H). ^{13}C NMR (151 MHz, DMSO-d_6) δ 173.28, 172.29, 153.16, 136.51, 132.77, 132.33, 131.95, 128.67, 127.74, 124.72, 124.47, 124.13, 122.93, 121.31, 118.64, 111.72, 110.59, 57.34, 53.70, 29.61, 28.53, 26.12, 26.05. HRMS (ESI/Q-TOF) *m/z*: $[M + H]^+$ Calcd for $C_{31}H_{31}BrN_4O_4S$ 635,1249; Found 635,1331 HPLC Ret. time 41.8 min, purity 96 % (254 nm) 95 % (214 nm).

4.4.10. Ethyl (R)-2-((S)-2-((E)-3-(2-(4-bromophenyl)thiazol-4-yl) acrylamido)-3-(1H-indol-3-yl)propanamido)-2-phenylacetate (12)

Compound **12** was synthesized following the procedure for **10**, from **5** and **9b.** Yield 84 %; ^{1}H NMR (600 MHz, $CDCl_3$) δ 8.06 (s, 1H), 7.86–7.77 (m, 2H), 7.62–7.53 (m, 3H), 7.36–7.29 (m, 3H), 7.15–7.07 (m, 3H), 6.91–6.77 (m, 3H), 5.43 (d, $J = 7.2$ Hz, 1H), 5.01 (td, $J = 7.9$, 5.5 Hz, 2H), 4.10 (ddq, $J = 46.8$, 10.8, 7.1 Hz, 2H), 3.37–3.32 (m, 1H), 3.20 (dd, $J = 14.5$, 8.0 Hz, 1H), 1.15 (t, $J = 7.1$ Hz, 3H). ^{13}C NMR (151 MHz, $CDCl_3$) δ 170.81, 170.43, 167.43, 166.17, 152.79, 136.14, 135.92, 133.61, 132.21, 132.07, 128.85, 128.45, 128.17, 127.34, 127.22, 124.86, 123.27, 122.87, 122.30, 121.25, 119.87, 118.80, 111.26, 110.13, 62.00, 56.64, 53.82, 50.79, 30.95, 28.32, 13.91. HRMS (ESI/Q-TOF) *m/z*: $[M + H]^+$ Calcd for $C_{33}H_{29}BrN_4O_4S$ 656,1093; Found 657,1161 HPLC Ret. time 44.012 min, purity 90 % (254 nm) 88 % (214 nm).

4.4.11. Tert-butyl 5-(4-bromophenyl) nicotinate (14)

5-(4-bromophenyl) nicotinic acid (0.250 g; 0.9026 mmol) and DMAP (0.0224 g; 0.1834 mmol were dissolved in THF and heated at reflux. Then, di-tert-butyl dicarbonate (0.4945 g; 2.2671 mmol) was dissolved in THF and added dropwise to the reaction. This mixture was refluxed for 4 h and monitored using TLC. Once the reaction was completed, it was allowed to cool down to rt and concentrated. Then, the residue was dissolved in MTBE and washed with water, 1 M phosphoric acid, demi-water, 10 % sodium carbonate solution and brine. Then the organic layer was dried using magnesium sulphate and concentrated to yield 14 (yield: 55 %). ^{1}H NMR (400 MHz, $CDCl_3$) δ 9.15 (d, $J = 2.0$ Hz, 1H), 8.93 (d, $J = 2.3$ Hz, 1H), 8.39 (t, $J = 2.0$ Hz, 1H), 7.68–7.60 (m, 2H), 7.53–7.45 (m, 2H), 1.63 (s, 9H).

4.4.12. Tert-butyl 5-(4-(furan-2-yl)phenyl)nicotinate (15)

14 (0.165 g; 0.4954 mmol), Pd(dppf)Cl_2 (0.041 g; 0.056 mmol) and sodium tert-butoxide (0.0532 g; 0.5536 mmol) were dissolved in THF/water 9:1 and heated at reflux under argon. After this, furan-2-boronic acid (0.0622 g; 0.5552 mmol) was added dropwise over 1 h and allowed to reflux overnight. Once TLC showed that the reaction was not proceeding anymore, the reaction was cooled to r. t. and concentrated. Then water was added and extracted using DCM, after which the organic layer was washed using brine, dried over magnesium sulphate, concentrated, and dried. Column chromatography was used to purify 2H using 30 % EtOAc/PE as eluent (yield: 58,6%) ^{1}H NMR (400 MHz, $CDCl_3$) δ 9.13 (d, $J = 2.0$ Hz, 1H), 9.00 (d, $J = 2.3$ Hz, 1H), 8.45 (t, $J = 2.2$ Hz, 1H), 7.84–7.77 (m, 2H), 7.69–7.61 (m, 2H), 7.54–7.49 (m, 1H), 6.74 (dd, $J = 3.4$, 0.8 Hz, 1H), 6.52 (dd, $J = 3.4$, 1.8 Hz, 1H), 1.64 (s, 9H).

4.4.13. 5-(4-(furan-2-yl)phenyl)nicotinic acid (16)

15 (0.0858 g; 0.0377 mmol) was dissolved in DCM (10 mL) and cooled in an ice bath, then TFA (1 mL) was added, and the mixture was allowed to stir overnight at r. t. Once TLC showed full deprotection, the mixture was concentrated, and column chromatography was used to purify **16** using 10 % MeOH, 89 % DCM and 1 % triethylamine (yield: 92 %). ^{1}H NMR (400 MHz, DMSO-d_6) δ 9.05 (s, 2H), 8.48 (s, 1H), 7.85 (s, 4H), 7.80 (d, $J = 1.8$ Hz, 1H), 7.07 (d, $J = 3.3$ Hz, 1H), 6.64 (dd, $J = 3.3$, 1.8 Hz, 1H).

4.4.14. N-methoxy-N-methyl-[1,1′-biphenyl]-4-carboxamide (17)

4-biphenylcarbonyl chloride (9.979 g; 46.19 mmol) and *N,O*-dimethylhydroxylamine (4.673 g; 47.91 mmol) were dissolved in DCM 200 mL and put in an ice bath. Then triethylamine (13 mL; 93.3 mmol) was added slowly, and the suspension was stirred overnight. Once TLC showed complete conversion, the reaction was quenched with a saturated ammonium chloride solution (20 mL) and stirred for 30 min. Then, the aqueous phase was extracted with DCM (2 x 150 mL), then washed with brine (150 mL). Subsequently, the organic phase was dried using magnesium sulphate, concentrated and dried. The product was purified using column chromatography with 30 % EtOAc in PE (yield: 81,7%).^{1}H NMR (400 MHz, $CDCl_3$) δ 7.82–7.74 (m, 2H), 7.67–7.58 (m, 4H), 7.51–7.42 (m, 2H), 7.42–7.34 (m, 1H), 3.60 (s, 3H), 3.39 (s, 3H).

4.4.15. [1,1′-biphenyl]-4-carbaldehyde (18)

17 (9.1 g; 37.7 mmol) was dissolved in THF and cooled down to −78℃ using dry ice. Then, a $LiAlH_4$ solution in THF (1 M, 44 mL; 44 mmol) was added in small portions over 1 h. After 1 h of stirring, the reaction was allowed to warm to 4℃ slowly and stirred overnight. The reaction was monitored using TLC using 50 % EtOAc in PE as an eluent. Once completed, the reaction was quenched with a 10 % potassium bisulphate solution at 4℃ and allowed to warm to r. t. Then, the product was concentrated, and water (100 mL) was added to the mixture after which it was extracted using EtOAc (three times 100 mL), and then the organic phase was washed using brine once. Subsequently, the organic layer was dried using magnesium sulphate and concentrated and dried to yield **18** (yield: 93,1%). ^{1}H NMR (400 MHz, $CDCl_3$) δ 10.06 (s, 1H), 8.00–7.92 (m, 2H), 7.80–7.72 (m, 2H), 7.68–7.62 (m, 2H), 7.53–7.45 (m, 2H), 7.45–7.40 (m, 1H).

4.4.16. 3-([1,1′-biphenyl]-4-yl)-3-aminopropanoic acid (19)

18 (6.4 g; 35.2 mmol), malonic acid (4.22 g; 40.6 mmol) and ammonium acetate (4.94 g; 70.3 mmol) were dissolved in ethanol. This was then refluxed overnight, after which a white precipitate was formed. The reaction was allowed to cool down to r. t., and the precipitate was collected by vacuum filtration and washed with ethanol. Then the precipitate was dried and analyzed (yield: 35.%). ^{1}H NMR (400 MHz, D_2O) δ 7.73 (t, $J = 8.0$ Hz, 4H), 7.53 (t, $J = 8.0$ Hz, 4H), 7.46 (d, $J = 8.0$ Hz, 1H), 4.34 (d, $J = 7.5$ Hz, 1H), 2.63 (d, $J = 7.5$ Hz, 2H).

4.4.17. Ethyl 3-([1,1′-biphenyl]-4-yl)-3-aminopropanoate (20)

19 (0.225 g; 1.057 mmol) was suspended in ethanol and cooled using an ice bath. Then thionyl chloride (0.09 mL; 9.2 mmol) was slowly added to the reaction, upon which a clear solution formed. This was refluxed for 3 h until TLC showed the reaction was completed. The reaction was cooled down to r. t., concentrated and purified using column chromatography using 70 % EtOAc/PE as an eluent, leading to a yield of 92 %.^{1}H NMR (400 MHz, $CDCl_3$) δ 8.91 (s, 2H), 7.68–7.53 (m, 4H), 7.50 (d, $J = 7.4$ Hz, 2H), 7.36 (dt, $J = 13.4$, 7.0 Hz, 3H), 4.80 (s, 1H), 4.12–3.93 (m, 2H), 3.30 (s, 1H), 3.09 (s, 1H), 1.10 (s, 3H).

4.4.18. Standard peptide coupling method for 21, 24, 25, 26, 27a and 27b

Peptide couplings were performed using the following procedure unless otherwise mentioned: 1 equiv of acid and 1.1 equiv of HATU were dissolved in DMF and 6 equiv of DIPEA was added. After stirring for 30 min a solution of 1.2 equiv of amine in DMF was added dropwise and the mixture was stirred for 48–120 h until TLC showed complete consumption of the acid. The reaction mixture was concentrated and co-evaporated 2-times with toluene followed by column chromatography (3:7 PE: EtOAc) to yield the coupling product.

4.4.19. Ethyl 3-([1,1′-biphenyl]-4-yl)-3-(5-(4-(furan-2-yl)phenyl) nicotinamido)propanoate (21)

16 (35 mg; 0.132 mmol), HATU (55.5 mg; 0.146 mmol), DIPEA (0.15 mL; 0.861 mmol) and **20** (46 mg; 0.171 mmol) were reacted using the standard peptide coupling method which resulted in a light-yellow

solid. (yield: 72 %) ^{1}H NMR (600 MHz, CD_3OD): δ 8.97 (d, J = 2.1 Hz, 1H), 8.92 (d, J = 2.3 Hz, 1H), 8.46 (t, J = 2.1 Hz, 1H), 7.83–7.79 (m, 2H), 7.71–7.67 (m, 2H), 7.62–7.56 (m, 4H), 7.55–7.50 (m, 3H), 7.43 (dd, J = 8.4, 7.0 Hz, 2H), 7.37–7.32 (m, 1H), 6.77 (dd, J = 3.4, 0.8 Hz, 1H), 6.52 (dd, J = 3.4, 1.8 Hz, 1H), 5.72 (dd, J = 8.1, 6.2 Hz, 1H), 4.15 (q, 2H), 3.18–2.96 (m, 2H), 1.22 (t, J = 7.1 Hz, 3H) ^{13}C NMR (151 MHz, CD_3OD): δ 171.34, 165.32, 153.06, 149.51, 146.31, 142.58, 140.69, 140.50, 139.66, 136.44, 134.92, 133.91, 131.24, 130.41, 128.71, 127.36, 127.33, 126.97, 126.91, 124.43, 111.81, 105.94, 61.04, 50.42, 40.23, 13.84. HRMS (ESI/Q-TOF) *m/z*: $[M + H]^+$ Calcd for $C_{33}H_{28}N_2O_4$ 517.2049; Found 517.2140 HPLC Ret. time 36 min purity 100 % (254 nm) 98 0.2% (214 nm).

4.4.20. Ethyl 3-(4-bromophenyl)-3-(5-(4-(furan-2-yl)phenyl) nicotinamido)propanoate (24)

16 (31.7 mg; 0.120 mmol) was dissolved in DMF (5 mL). A solution of DIPEA (0.15 mL; 0.861 mmol), HATU (53 mg; 0.139 mmol) and HOBt (3.34 mg; 0.025 mmol) in DMF were added over 30 min. After, a solution of **22** (47 mg; 0.173 mmol) in DMF (5 mL) was added and stirred overnight. Then, the reaction mixture was concentrated, co-evaporated 2-times with toluene followed by column chromatography (3:7 PE: EtOAc) of the residue which resulted in a yellow solid. (Yield: 39 %) ^{1}H NMR (600 MHz, CD_3OD) δ 8.93 (s, 2H), 8.41 (s, 1H), 7.80–7.75 (m, 2H), 7.67–7.62 (m, 2H), 7.49 (dd, J = 1.9, 0.7 Hz, 1H), 7.47–7.41 (m, 3H), 7.32–7.26 (m, 2H), 6.73 (dd, J = 3.4, 0.8 Hz, 1H), 6.48 (dd, J = 3.4, 1.8 Hz, 1H), 5.57 (dd, J = 8.1, 6.4 Hz, 1H), 4.09 (q, 2H), 3.04–2.85 (m, 2H), 1.17 (t, J = 7.1 Hz, 3H). ^{13}C NMR (151 MHz, CD_3OD) δ 170.98, 165.33, 153.04, 149.44, 146.20, 142.59, 139.89, 134.89, 133.97, 132.38, 131.74, 131.29, 128.40, 127.34, 124.43, 121.55, 111.80, 105.95, 61.05, 50.21, 40.04, 13.80. HRMS (ESI/Q-TOF) *m/z*: $[M + H]^+$ Calcd for $C_{27}H_{23}BrN_2O_4$ 519.08419; Found 519.0898 HPLC Ret.time 38.9 min purity 96 % (254 nm) 93.5 % (214 nm).

4.4.21. Ethyl 3-(4-bromophenyl)-3-(5-(4-bromophenyl)nicotinamido) propanoate (25)

5-(4-bromophenyl)nicotinic acid (41 mg; 0.147 mmol), HATU (62 mg; 0.163 mmol), DIPEA (0.15 mL; 0.861 mmol) and **22** (44.3 mg; 0.163 mmol) were reacted using the standard peptide coupling method which gave a yellow solid. (yield: 37 %) ^{1}H NMR (600 MHz, CD_3OD): δ 8.96 (d, J = 2.1 Hz, 1H), 8.87 (d, J = 2.2 Hz, 1H), 8.39 (t, J = 2.1 Hz, 1H), 7.67–7.62 (m, 2H), 7.56–7.51 (m, 2H), 7.50–7.47 (m, 2H), 7.36–7.31 (m, 2H), 5.61 (dd, J = 8.1, 6.4 Hz, 1H), 4.13 (q, J = 7.1 Hz, 2H), 3.08–2.90 (m, 2H), 1.21 (t, J = 7.1 Hz, 3H). ^{13}C NMR (151 MHz, CD_3OD): δ 171.39, 165.50, 149.92, 147.05, 140.17, 136.20, 135.66, 134.39, 132.72, 132.09, 130.61, 129.03, 128.74, 123.53, 121.91, 61.42, 50.53, 40.32, 14.16. HRMS (ESI/Q-TOF) *m/z*: $[M + H]^+$ Calcd for $C_{23}H_{20}BrN_2O_3$ 531.2049; Found 532.9893 HPLC Ret. time 38.9 min, purity 95 % (254 nm) 94.7 % (214 nm).

4.4.22. Ethyl 3-([1,1′-biphenyl]-4-yl)-3-(5-(4-bromophenyl)nicotinamido) propanoate (26)

5-(4-bromophenyl)nicotinic acid (100 mg; 0.360 mmol), HATU (163 mg; 0.429 mmol), DIPEA (0.15 mL; 0.861 mmol) and **20** (110 mg; 0.409 mmol) were reacted using the standard peptide coupling method resulting in a white solid. (yield: 40 %) ^{1}H NMR (600 MHz, $CDCl_3$): δ 9.03 (d, J = 2.0 Hz, 1H), 8.88 (d, J = 2.2 Hz, 1H), 8.31 (t, J = 2.2 Hz, 1H), 7.98 (d, J = 8.2 Hz, 1H), 7.62–7.57 (m, 2H), 7.57–7.52 (m, 4H), 7.47–7.39 (m, 6H), 7.37–7.31 (m, 1H), 5.70 (dt, J = 8.2, 5.8 Hz, 1H), 4.13 (q, J = 7.1 Hz, 2H), 3.11–2.96 (m, 2H), 1.20 (t, J = 7.1 Hz, 3H) ^{13}C NMR (151 MHz, $CDCl_3$): δ 171.62, 164.66, 150.48, 146.75, 140.78, 140.47, 139.26, 135.65, 135.58, 133.51, 132.42, 130.04, 128.83, 128.76, 127.54, 127.47, 127.05, 126.78, 123.15, 77.30, 77.09, 76.88, 61.15, 50.00, 39.72, 14.12. HRMS (ESI/Q-TOF) *m/z*: $[M + H]^+$ Calcd for $C_{29}H_{25}BrN_2O_3$ 529.1049; Found 529.1120 HPLC Ret. time 41mn, purity 100 % (254 nm) 100 % (214 nm).

4.4.23. (R)-ethyl 3-(5-(4-(furan-2-yl)phenyl)nicotinamido)-3-phenylpropanoate) (27a)

16 (50 mg; 0.188 mmol), HATU (79.5 mg; 0.209 mmol), DIPEA (0.2 mL; 1.15 mmol), HOBt (0.05 mL; 0.025 mmol) in DMF and *(R)*-ethyl 3-amino-3-phenylpropanoate (42 mg; 0.217 mmol) were reacted using the standard peptide coupling method resulting in a yellow solid. (yield: 35 %) ^{1}H NMR (600 MHz, $CDCl_3$): δ 8.99 (d, 3H), 8.52 (s, 1H), 8.13 (d, J = 8.7 Hz, 1H), 7.77 (d, J = 8.6 Hz, 2H), 7.61 (d, J = 8.3 Hz, 2H), 7.51 (d, J = 1.7 Hz, 1H), 7.41–7.30 (m, 4H), 7.27 (tt, J = 6.6, 2.5 Hz, 1H), 6.74 (d, J = 3.4 Hz, 1H), 6.51 (dt, J = 3.2, 1.4 Hz, 1H), 5.65 (q, J = 6.4 Hz, 1H), 4.11 (q, J = 7.1 Hz, 2H), 3.13–2.90 (m, 2H), 1.18 (t, J = 7.1 Hz, 3H). ^{13}C NMR (151 MHz, $CDCl_3$): δ 171.50, 163.73, 152.94, 147.64, 143.99, 142.78, 140.19, 137.31, 135.52, 134.06, 131.67, 131.12, 128.86, 127.92, 127.45, 126.40, 124.64, 111.96, 106.31, 61.11, 50.49, 39.77, 14.07 HRMS (ESI/Q-TOF) *m/z*: $[M + H]^+$ Calcd for $C_{27}H_{24}N_2O_4$ 440.1736; Found 441.1811 HPLC Ret. time 35.5 min, purity 100 % (254 nm) 100 % (214 nm).

4.4.24. (S)-ethyl 3-phenyl-3-(5-phenylnicotinamido)propanoate (27b)

16 (50 mg; 0.188 mmol), HATU (79,5 mg; 0.209 mmol), DIPEA (0.2 mL; 1.115 mmol), HOBt (0,05 mL; 0.025 mmol) in DMF and *(S)*-ethyl 3-amino-3-phenylpropanoate (41.3 mg; 0.214 mmol) were reacted using the standard peptide coupling method resulting yielding to a yellow solid. (Yield: 75 %) ^{1}H NMR (600 MHz, $CDCl_3$) δ 8.99 (d, J = 2.1 Hz, 1H), 8.91 (d, J = 2.2 Hz, 1H), 8.31 (t, J = 2.1 Hz, 1H), 7.97–7.84 (m, 1H), 7.57 (ddd, J = 8.2, 2.3, 1.3 Hz, 2H), 7.50–7.44 (m, 2H), 7.44–7.39 (m, 1H), 7.39–7.36 (m, 2H), 7.33 (dd, J = 8.3, 6.9 Hz, 2H), 7.27 (tt, J = 6.6, 1.3 Hz, 1H), 5.66 (dt, J = 8.2, 5.8 Hz, 1H), 4.10 (q, J = 7.2 Hz, 2H), 3.08–2.90 (m, 2H), 1.17 (t, J = 7.1 Hz, 3H). ^{13}C NMR (151 MHz, $CDCl_3$) δ 171.53, 164.81, 150.73, 146.50, 140.29, 136.76, 136.66, 133.55, 129.97, 129.22, 128.82, 128.59, 127.83, 127.22, 126.34, 61.04, 50.18, 39.81, 14.09. HRMS (ESI/Q-TOF) *m/z*: $[M + H]^+$ Calcd for $C_{27}H_{24}N_2O_4$ 440.1736; Found 441.1811 HPLC Ret. time 35.6 min, purity 100 % (254 nm) 100 % (214 nm).

4.4.25. N-(1-([1,1′-biphenyl]-4-yl)-3-(methylamino)-3-oxopropyl)-5-(4-(furan-2-yl)phenyl)nicotinamide (10115)

Compound **21** (9 mg; 0.017 mmol) was suspended in a solution of $MeNH_2$ in MeOH (40 %, 0.5 mL) in a vial and heated to 80 ℃ for 3 h using a microwave irradiation. The mixture was concentrated and purified using preparative HPLC (yield: 69 %) ^{1}H NMR (600 MHz, DMSO-d_6): δ 9.21 (d, J = 8.1 Hz, 1H), 9.08 (d, J = 2.2 Hz, 1H), 8.99 (d, J = 2.1 Hz, 1H), 8.49 (t, J = 2.2 Hz, 1H), 7.93–7.84 (m, 5H), 7.80 (dd, J = 1.8, 0.7 Hz, 1H), 7.64 (ddt, J = 10.3, 8.5, 1.8 Hz, 4H), 7.53–7.48 (m, 2H), 7.48–7.42 (m, 2H), 7.38–7.32 (m, 1H), 7.08 (dd, J = 3.3, 0.7 Hz, 1H), 6.64 (dd, J = 3.4, 1.8 Hz, 1H), 5.54 (q, J = 7.6 Hz, 1H), 2.75 (dd, J = 7.4, 1.9 Hz, 2H), 2.55 (d, J = 4.5 Hz, 3H). ^{13}C NMR (151 MHz, DMSO-d_6): δ 169.68, 164.00, 152.45, 149.69, 147.52, 143.39, 142.02, 139.93, 138.89, 135.10, 134.53, 132.48, 130.37, 130.01, 128.93, 127.58, 127.36, 127.20, 126.64, 126.61, 124.13, 112.31, 106.77, 50.41, 41.90, 25.51. HRMS (ESI/Q-TOF) *m/z*: $[M + H]^+$ Calcd for $C_{32}H_{27}N_3O_3$ 501.2052; Found 502.2118 HPLC Ret. time 35.48 min, purity 97 % (254 nm) 95 % (214 nm).

CRediT authorship contribution statement

Cyril Balsollier: Writing – original draft, Visualization, Methodology, Investigation, Formal analysis, Data curation, Writing – review & editing. **Simon Bijkerk:** Investigation. **Arjan de Smit:** Investigation. **Kevin van Eekelen:** Investigation. **Krištof Bozovičar:** Investigation. **Dirk Husstege:** Investigation. **Tihomir Tomašič:** Formal analysis, Methodology, Supervision, Writing – review & editing. **Marko Anderluh:** Conceptualization, Formal analysis, Funding acquisition, Methodology, Project administration, Supervision, Validation, Writing – review & editing. **Roland J. Pieters:** Writing – review & editing, Supervision, Methodology, Funding acquisition, Conceptualization.

Declaration of competing interest

The authors declare that they have no known competing financial interests or personal relationships that could have appeared to influence the work reported in this paper.

Acknowledgements

This work has been funded by the European Union's Horizon 2020 research and innovation programme under the Marie Skłodowska Curie grant agreement No 765581 (PhD4GlycoDrug Innovative Training Network). The DELopen library and the off-DNA synthesis of hits were provided by WuXi AppTec. The academic license for OpenEye software was kindly provided by OpenEye Scientific Software Inc. to the laboratory of Roland Pieters.

Appendix A. Supplementary data

Supplementary data to this article (^{1}H and ^{13}C NMR spectra of the target compounds and theintermediates) can be found online at https://doi.org/10.1016/j.bioorg.2024.107321.

References

[1] L.K. Abramowitz, J.A. Hanover, T cell development and the physiological role of O-GlcNAc, FEBS Lett 592 (2018) 3943–3949, https://doi.org/10.1002/1873-3468.13159.
[2] V. Makwana, P. Ryan, B. Patel, S.A. Dukie, S. Rudrawar, Essential role of O-GlcNAcylation in stabilization of oncogenic factors, Biochim Biophys Acta Gen Subj 2019 (1863) 1302–1317, https://doi.org/10.1016/j.bbagen.2019.04.002.
[3] W.A. Lubas, M. Smith, C.M. Starr, J.A. Hanover, Analysis of Nuclear pore protein p62 glycosylation, Biochemistry 34 (1995) 1686–1694, https://doi.org/10.1021/bi00005a025.
[4] K. Vosseller, L. Wells, M.D. Lane, G.W. Hart, Elevated nucleocytoplasmic glycosylation by O-GlcNAc results in insulin resistance associated with defects in akt activation in 3T3-L1 adipocytes, Proc Natl Acad Sci U S A 99 (2002) 5313–5318, https://doi.org/10.1073/pnas.072072399.
[5] S.B. Peterson, G.W. Hart, New insights: a role for O-GlcNAcylation in diabetic complications, Crit Rev Biochem Mol Biol 51 (2016) 150–161, https://doi.org/10.3109/10409238.2015.1135102.
[6] J. Ma, G.W. Hart, Protein *O* -GlcNAcylation in diabetes and diabetic complications, Expert Rev Proteomics 10 (2013) 365–380, https://doi.org/10.1586/14789450.2013.820536.
[7] S.A. Yuzwa, X. Shan, M.S. Macauley, T. Clark, Y. Skorobogatko, K. Vosseller, D. J. Vocadlo, Increasing O-GlcNAc slows neurodegeneration and stabilizes tau against aggregation, Nat Chem Biol 8 (2012) 393–399, https://doi.org/10.1038/nchembio.797.
[8] K. Iqbal, F. Liu, C.-X. Gong, I. Grundke-Iqbal, Tau in Alzheimer disease and related tauopathies, Curr Alzheimer Res 7 (2010) 656–664, https://doi.org/10.2174/156720510793611592.
[9] A. Hatori, Y. Fujii, Y. Kawase-Koga, T. Ogasawara, J. Chikira, S. Minami, D. Yamakawa, D. Chikazu, VCAM-1 and GFPT-2: predictive markers of osteoblast differentiation in human dental pulp stem cells, Bone 166 (2023) 116575, https://doi.org/10.1016/j.bone.2022.116575.
[10] S. Özcan, S.S. Andrali, J.E.L. Cantrell, Modulation of transcription factor function by O-GlcNAc modification, Biochim Biophys Acta Gene Regul Mech 1799 (2010) 353–364, https://doi.org/10.1016/j.bbagrm.2010.02.005.
[11] P. Jóźwiak, P. Ciesielski, P.K. Zakrzewski, K. Kozal, J. Oracz, G. Budryn, D. Żyżelewicz, S. Flament, A.-S. Vercoutter-Edouart, F. Bray, T. Lefebvre, A. Krześlak, Mitochondrial O-GlcNAc transferase Interacts with and modifies many proteins and its up-regulation affects mitochondrial function and Cellular energy homeostasis, Cancers (basel) 13 (2021), https://doi.org/10.3390/cancers13122956.
[12] C.M. Joiner, H. Li, J. Jiang, S. Walker, Structural characterization of the O-GlcNAc cycling enzymes: insights into substrate recognition and catalytic mechanisms, Curr Opin Struct Biol 56 (2019) 97–106, https://doi.org/10.1016/j.sbi.2018.12.003.
[13] M.B. Lazarus, Y. Nam, J. Jiang, P. Sliz, S. Walker, Structure of human O-GlcNAc transferase and its complex with a peptide substrate, Nature 469 (2011) 564–569, https://doi.org/10.1038/nature09638.
[14] E.J. Kim, O -GlcNAc transferase: structural characteristics, catalytic mechanism and small molecule inhibitors, ChemBioChem (2020), https://doi.org/10.1002/cbic.202000194.
[15] H.G. Selnick, J.F. Hess, C. Tang, K. Liu, J.B. Schachter, J.E. Ballard, J. Marcus, D. J. Klein, X. Wang, M. Pearson, M.J. Savage, R. Kaul, T.S. Li, D.J. Vocadlo, Y. Zhou, Y. Zhu, C. Mu, Y. Wang, Z. Wei, C. Bai, J.L. Duffy, E.J. McEachern, Discovery of MK-8719, a potent O-GlcNAcase inhibitor as a potential treatment for tauopathies, J Med Chem 62 (2019) 10062–10097, https://doi.org/10.1021/acs.jmedchem.9b01090.
[16] H.E. Lee, D. Lim, J.Y. Lee, S.M. Lim, A.N. Pae, Recent tau-targeted clinical strategies for the treatment of Alzheimer's disease, Future Med Chem 11 (2019) 1845–1848, https://doi.org/10.4155/fmc-2019-0151.
[17] S. Wang, D.L. Shen, D. Lafont, A.-S. Vercoutter-Edouart, M. Mortuaire, Y. Shi, O. Maniti, A. Girard-Egrot, T. Lefebvre, B.M. Pinto, D. Vocadlo, S. Vidal, Design of glycosyltransferase inhibitors targeting human O-GlcNAc transferase (OGT), Medchemcomm 5 (2014) 1172, https://doi.org/10.1039/C4MD00063C.
[18] V.S. Borodkin, M. Schimpl, M. Gundogdu, K. Rafie, H.C. Dorfmueller, D. A. Robinson, D.M.F. van Aalten, Bisubstrate UDP–peptide conjugates as human O-GlcNAc transferase inhibitors, Biochem. J. 457 (2014) 497–502, https://doi.org/10.1042/BJ20131272.
[19] K. Rafie, A. Gorelik, R. Trapannone, V.S. Borodkin, D.M.F. Van Aalten, Thio-linked UDP-peptide conjugates as O-GlcNAc transferase inhibitors, Bioconjug Chem 29 (2018) 1834–1840, https://doi.org/10.1021/acs.bioconjchem.8b00194.
[20] V. Makwana, P. Ryan, A.K. Malde, S. Anoopkumar-Dukie, S. Rudrawar, Bisubstrate ether-linked uridine-peptide conjugates as O-GlcNAc transferase inhibitors, ChemMedChem 16 (2021) 477–483, https://doi.org/10.1002/cmdc.202000582.
[21] M. Weiss, E.M. Loi, M. Sterle, C. Balsollier, T. Tomašič, R.J. Pieters, M. Gobec, M. Anderluh, New quinolinone O-GlcNAc transferase inhibitors based on fragment growth, Front Chem 9 (2021) 666122, https://doi.org/10.3389/fchem.2021.666122.
[22] C. Balsollier, T. Tomašič, D. Yasini, S. Bijkerk, M. Anderluh, R.J. Pieters, Design of OSMI-4 analogs using scaffold hopping: investigating the importance of the uridine mimic in the binding of OGT inhibitors, ChemMedChem (2023), https://doi.org/10.1002/cmdc.202300001.
[23] H. Zhang, T. Tomašič, J. Shi, M. Weiss, R. Ruijtenbeek, M. Anderluh, R.J. Pieters, Inhibition of: O -GlcNAc transferase (OGT) by peptidic hybrids, Medchemcomm 9 (2018) 883–887, https://doi.org/10.1039/c8md00115d.
[24] R.F. Ortiz-Meoz, J. Jiang, M.B. Lazarus, M. Orman, J. Janetzko, C. Fan, D. Y. Duveau, Z.-W. Tan, C.J. Thomas, S. Walker, A small molecule that inhibits OGT activity in cells, ACS Chem Biol 10 (2015) 1392–1397, https://doi.org/10.1021/acschembio.5b00004.
[25] S.E.S. Martin, Z.-W. Tan, H.M. Itkonen, D.Y. Duveau, J.A. Paulo, J. Janetzko, P. L. Boutz, L. Törk, F.A. Moss, C.J. Thomas, S.P. Gygi, M.B. Lazarus, S. Walker, Structure-based evolution of low Nanomolar O-GlcNAc transferase inhibitors, J Am Chem Soc 140 (2018) 13542–13545, https://doi.org/10.1021/jacs.8b07328.
[26] X. Shan, R. Jiang, D. Gou, J. Xiang, P. Zhou, J. Xia, K. Wang, A. Huang, N. Tang, L. Huang, Identification of a diketopiperazine-based O-GlcNAc transferase inhibitor sensitizing hepatocellular carcinoma to CDK9 inhibition, FEBS Journal (2023), https://doi.org/10.1111/febs.16877.
[27] Y. Wang, J. Zhu, L. Zhang, Discovery of cell-permeable O-GlcNAc transferase inhibitors via tethering in situ click chemistry, J Med Chem 60 (2017) 263–272, https://doi.org/10.1021/acs.jmedchem.6b01237.
[28] Y. Liu, Y. Ren, Y. Cao, H. Huang, Q. Wu, W. Li, S. Wu, J. Zhang, Discovery of a low toxicity O-GlcNAc transferase (OGT) inhibitor by structure-based virtual screening of natural products, Sci Rep 7 (2017) 1–11, https://doi.org/10.1038/s41598-017-12522-0.
[29] E.M. Loi, M. Weiss, S. Pajk, M. Gobec, T. Tomašič, R.J. Pieters, M. Anderluh, Intracellular hydrolysis of small-molecule O-linked N-Acetylglucosamine transferase inhibitors differs among cells and is not required for its inhibition, Molecules 25 (2020) 3381, https://doi.org/10.3390/molecules25153381.
[30] A. Gironda-Martínez, E.J. Donckele, F. Samain, D. Neri, DNA-encoded chemical Libraries: a comprehensive review with succesful stories and future challenges, ACS Pharmacol Transl Sci 4 (2021) 1265–1279, https://doi.org/10.1021/acsptsci.1c00118.
[31] M. Proj, K. Bozovičar, M. Hrast, R. Frlan, S. Gobec, DNA-encoded library screening on two validated enzymes of the peptidoglycan biosynthetic pathway, Bioorg Med Chem Lett 73 (2022) 30–33, https://doi.org/10.1016/j.bmcl.2022.128915.
[32] L.H. Yuen, R.M. Franzini, Achievements, challenges, and opportunities in DNA-encoded Library Research: an academic point of view, ChemBioChem 18 (2017) 829–836, https://doi.org/10.1002/cbic.201600567.
[33] M. Song, G.T. Hwang, DNA-encoded Library screening as Core platform Technology in Drug Discovery: its synthetic method development and applications in DEL synthesis, J Med Chem 63 (2020) 6578–6599, https://doi.org/10.1021/acs.jmedchem.9b01782.
[34] S. Qin, L. Feng, Q. Zhao, Z. Yan, X. Lyu, K. Li, B. Mu, Y. Chen, W. Lu, C. Wang, Y. Suo, J. Yue, M. Cui, Y. Li, Y. Zhao, Z. Duan, J. Zhu, X. Lu, Discovery and optimization of WDR5 inhibitors via Cascade Deoxyribonucleic acid-encoded Library selection approach, J Med Chem 67 (2024) 1079–1092, https://doi.org/10.1021/acs.jmedchem.3c01463.
[35] X. Wen, M. Zhang, Z. Duan, Y. Suo, W. Lu, R. Jin, B. Mu, K. Li, X. Zhang, L. Meng, Y. Hong, X. Wang, H. Hu, J. Zhu, W. Song, A. Shen, X. Lu, Discovery, SAR study of GST inhibitors from a novel Quinazolin-4(1H)-one focused DNA-encoded Library, J Med Chem 66 (2023) 11118–11132, https://doi.org/10.1021/acs.jmedchem.2c02129.
[36] D. Guan, J. Liu, F. Chen, J. Li, X. Wang, W. Lu, Y. Suo, F. Tang, L. Lan, X. Lu, W. Huang, A vancomycin-templated DNA-encoded Library for combating drug-resistant bacteria, J Med Chem (2023), https://doi.org/10.1021/acs.jmedchem.3c02197.
[37] G. Hartman, P. Humphries, R. Hughes, A. Ho, R. Montgomery, A. Deshpande, M. Mahanta, S. Tronnes, S. Cowdin, X. He, F. Liu, L. Zhang, C. Liu, D. Dou, J. Li, A. Spasic, R. Coll, M. Marleaux, I.V. Hochheiser, M. Geyer, P. Rubin, K. Fortney, K. Wilhelmsen, The discovery of novel and potent indazole NLRP3 inhibitors enabled by DNA-encoded library screening, Bioorg Med Chem Lett 102 (2024), https://doi.org/10.1016/j.bmcl.2024.129675.

[38] DELopen available online: https://delopen.org/ (accessed 13 December 2023), (n. d.).
[39] M.G. Alteen, C. Gros, R.W. Meek, D.A. Cardoso, J.A. Busmann, G. Sangouard, M. C. Deen, H.Y. Tan, D.L. Shen, C.C. Russell, G.J. Davies, P.J. Robinson, A. McCluskey, D.J. Vocadlo, A direct fluorescent activity assay for Glycosyltransferases enables convenient high-throughput screening: application to O-GlcNAc transferase, Angew. Chem. Int. Ed. Engl. 59 (2020) 9601–9609, https://doi.org/10.1002/anie.202000621.
[40] M.B. Lazarus, J. Jiang, V. Kapuria, T. Bhuiyan, J. Janetzko, W.F. Zandberg, D. J. Vocadlo, W. Herr, S. Walker, HCF-1 is cleaved in the active site of O-GlcNAc transferase, Science 342 (2013) 1235–1239, https://doi.org/10.1126/science.1243990.
[41] M. McGann, FRED pose prediction and virtual screening accuracy, J Chem Inf Model 51 (2011) 578–596, https://doi.org/10.1021/ci100436p.
[42] M. McGann, FRED and HYBRID docking performance on standardized datasets, J Comput Aided Mol Des 26 (2012) 897–906, https://doi.org/10.1007/s10822-012-9584-8.
[43] Y.K. Abhale, A. Shinde, M. Shelke, L. Nawale, D. Sarkar, P.C. Mhaske, Synthesis of new 2-(thiazol-4-yl)thiazolidin-4-one derivatives as potential anti-mycobacterial agents, Bioorg Chem 115 (2021) 105192, https://doi.org/10.1016/j.bioorg.2021.105192.